Materials Today Bio 31 (2025) 101552

Contents lists available at ScienceDirect

Materials Today Bio

journal homepage: www.journals.elsevier.com/materials-today-bio

Improving ferroptosis-mediated immunotherapy for colorectal cancer through lysosome-targeted photodynamic therapy

Zhian Chen [a,1], Yutong Wang [b,1], Zhenhao Li [b,1], Meijuan Chen [c], Yingshi Li [d], Chuyue Lu [d], Zhenyu Lin [d], Hua Zheng [e,**], Lujia Chen [f,***], Qianbing Zhang [d,*]

[a] Zhongshan City People's Hospital, Zhongshan, 528403, China
[b] The First School of Clinical Medicine, Southern Medical University, Guangzhou, 510515, China
[c] State Key Laboratory of Organ Failure Research, Guangdong Provincial Key Laboratory of Viral Hepatitis Research, Department of Hepatology Unit and Infectious Diseases, Nanfang Hospital, Southern Medical University, Guangzhou, 510515, China
[d] Cancer Research Institute, School of Basic Medical Sciences, Southern Medical University, Guangzhou, Guangdong, 510515, China
[e] Department of Cardiology, Nanfang Hospital, Southern Medical University, Guangzhou, 510515, China
[f] Breast Center, Department of General Surgery, Nanfang Hospital, Southern Medical University, Guangzhou, China

ARTICLE INFO

Keywords:
Photodynamic therapy
Lysosomal targeting
Ferroptosis
Autophagy inhibition
Immunogenic cell death

ABSTRACT

Lysosomes is emerging as a promising therapeutic target for improving immunotherapy, which dysfunction would trigger lysosomal membrane permeabilization increase and subsequent leakage of reduced iron, which contributed to ferroptosis through cell-intrinsic Fenton chemistry. However, the integrity of lysosomal membranes is not susceptible to disrupt, owing to the presence of several Endo-lysosomal damage-response mechanisms. Herein, we developed a lysosome-targeted photosensitizer (TLA), which possessed robust light stability, good bio-compatibility, and high photodynamic therapy (PDT) effect. Upon internalized by cancer cells, TLA was specifically accumulated in lysosome, and which would destroy the integrity of lysosomal membranes and inhibit protective autophagy upon exposure to light irradiation. Subsequently, the cancer cells were suffered from ferroptosis through triggering cell-intrinsic Fenton chemistry and mitochondrial dysfunction, which would release damage-associated molecular pattern molecules (DAMPs) to induce immunogenic cell death and remodel immunosuppressive tumor microenvironment. Notably, combined with PD-L1 antibody and TLA could greatly potentiate the immune response and exhibit highest anti-tumor effects. In summary, this novel lysosome-targeted photosensitizer could serve as a promising strategy for the treatment of colorectal cancer.

1. Introduction

Immunotherapy, which could trigger inherent immune response to eliminate cancer cells, has revolutionized the treatment of various malignancies [1,2]. By blocking inhibitory signal and reactivating the functional-suppressed tumor infiltrating T lymphocytes (TILs), immune checkpoint inhibitors (ICIs) have achieved several clinical successes, highlighting its potential in cancer treatment. However, colorectal cancer (CRC) is known as "cold tumor" with less infiltration of TILs within its tumor micro-environment (TME), making them less responsive to immunotherapy [2,3]. Numerous evidences display that solid tumors tend to become resistant to ICIs by acquiring defects in the antigenicity of tumor cells and antigen presentation of dendritic cells (DCs) [4]. Therefore, the release of tumor antigen and the recruitment of immune cells are key determinants to destroy immunological tolerance and improve anticancer immune responses.

Ferroptosis is a type of iron and lipo-toxicity dependent regulated cell death, caused by the imbalance between the levels of oxidants and antioxidants [5,6]. Accumulating studies have revealed that OH· generated in Fe^{2+}-catalyzed Fenton reaction could cause lipid peroxidation and membrane damage, which are central biochemical event leading to ferroptosis [7,8]. Notably, ferroptosis not only effectively inhibits tumor growth, but occurs with immunogenic cell death (ICD) and reprogramming of TME [9–11]. Accompanied by the exposure and

* Corresponding author.
** Corresponding author.
*** Corresponding author.
E-mail addresses: gzhzmd@126.com (H. Zheng), dr_chenlj@smu.edu.cn (L. Chen), carl@smu.edu.cn (Q. Zhang).
[1] *Zhian Chen*, *Yutong Wang*, and *Zhenhao Li* contributed equally to this work.

https://doi.org/10.1016/j.mtbio.2025.101552
Received 16 November 2024; Received in revised form 10 January 2025; Accepted 3 February 2025
Available online 4 February 2025

release of DAMPs, ferroptosis-induced ICD helps to recruit and activate of antigen-presenting cells, as well as initiate of adaptive immune responses. To date, numerous iron-based nanocomposites, including iron-organic frameworks and iron oxide nanoparticles, have been widely applied as ferroptosis agents to promote lipid peroxidation (LPO) accumulation through triggering Fenton reaction, thereby causing cancer cell death and immune activation [12–14]. However, emerging studies identified that these exogenous iron-based inorganic nanomaterials would also elevate irons concentration within normal tissues, accompanied with serious side effects [11,15]. Therefore, specifically modulate Fenton reaction in cancer cell with metal-free molecular agents might be a novel and effective strategy.

Lysosome are important iron storage hubs and closely related to the maintenance of intracellular iron homeostasis [16]. Accumulated researches demonstrated that increased lysosomal membrane permeabilization might initiate or amplify cell death signaling of ferroptosis [17–19]. Besides, lysosome is the main organelle for autophagy. Emerging researches suggested that lysosome-mediated protective autophagy could inhibit ferroptosis within cancer cells by removing damaged or oxidized LPO [20]. Actually, owing to presence of protective autophagy, the ferroptosis-stimulatory nanomaterials were internalized and then disintegrated in lysosomes of tumor cells [21,22]. In line with this notion, the impairing autophagic process with quinacrine enhanced the response of the glioblastoma stem-like cells to temozolomide, by igniting ferroptosis [23]. Similarly, transferrin receptor (TfRC), which is critical for the iron import of cells, could be degraded via lysosome-mediated autophagy. Treatment with autophagic inhibitor chloroquine, TfRC was accumulated and consequently resulted in an elevated level of intracellular Fe^{2+}, then promoting ferroptosis [24]. Taken together, lysosome may be promising targets for triggering endogenous iron overload, so as to induce tumor ferroptosis.

Herein, we develop a lysosomal-targeted photosensitizer to trigger a "domino-effect" endogenous iron burst. This NIR photosensitizer is a "D-π-A" structured organic small molecule (TLA); in particular, the π bridge is thiophene, while the electron-donating group and electron-withdrawing unit are triphenylamine and rhodanic, respectively. Compared with hundreds of photosensitizers applied for PDT, TLA specifically targeted lysosome, displaying robust light stability, good biocompatibility, high photothermal conversion efficiency. Mechanically, lysosome was selectively damaged with TLA-mediated PDT, causing lysosome leaky and autophagy inhibition, which further enhanced cell-intrinsic Fenton reactions and amplified cellular ferroptosis. Moreover, in vitro and in vivo experiment demonstrated that TLA-mediated PDT could induce strong anti-tumor immune response and promote the transition from "cold" to "hot" tumors, which exhibited a synergistic efficacy in combination with PD-L1 antibody (A-PD-L1) therapy (Scheme 1). Collectively, TLA has the potential to boost ferroptosis and trigger a robust immune response against tumors, which providing a novel therapeutic strategy for immunotherapy-resistant tumors.

2. Results

2.1. Synthesis and physical properties of TLA

Base on the preliminary research, we optimize the structure of TTM and developed a novel photosensitizer TLA [25]. In brief, TLA was synthesized through a reaction between the 5-(4-(diphenylamino) phenyl) thiophene-2-carbaldehyde with rhodanic as shown in Fig. 1A and Fig. S1 (Supporting Information). The synthetic routine, NMR, and mass spectra are provided in Figs. S2–6 (Supporting Information).

Additionally, the optical properties of TLA were characterized via UV absorption and fluorescence spectra. As depicted in Fig. 1B, TLA exhibited an absorption maximum at 505 nm in water containing 0.1 % DMSO ascribed to intramolecular charge transfer (ICT) effect from the triphenylamine moiety to the rhodanic group. The absorption spread broadly in the visible-light range from 400 to 600 nm, indicating that TLA can be activated using a white-light lamp. Moreover, the emission maximum of TLA is located at around 695 nm, which belongs to the near-infrared region. More importantly, TLA emits NIR fluorescence with a large Stokes shift of 190 nm, avoiding molecular self-absorption and giving great advantages for bioimaging applications.

The fluorescence probing approach was utilized to assess the TLA' capacity to generate ROS in vitro. By using 2′,7′-dichlorodihydrofluorescein (DCFH), a commercial indicator for all general forms of ROS, we first assessed the ROS generation of TLA. As depicted in Fig. 1C–D, when exposed to light (400–700 nm white LED light, 60 mW/cm^2) for 60 s, the solution of DCFH containing TLA exhibits an approximately 12.1-fold fluorescence amplification at 522 nm, showing the efficient production of ROS. Then, to identify $^1O_2$, 9,10-anthracenediyl- bis (methylene)-dimalonic acid (ABDA) was employed as a singlet oxygen indicator. After the 60s of light irradiation on an ABDA solution containing TLA, the absorbance of ABDA disappeared (Fig. 1E; Fig. S7, Supporting Information), suggesting the generation of $^1O_2$.

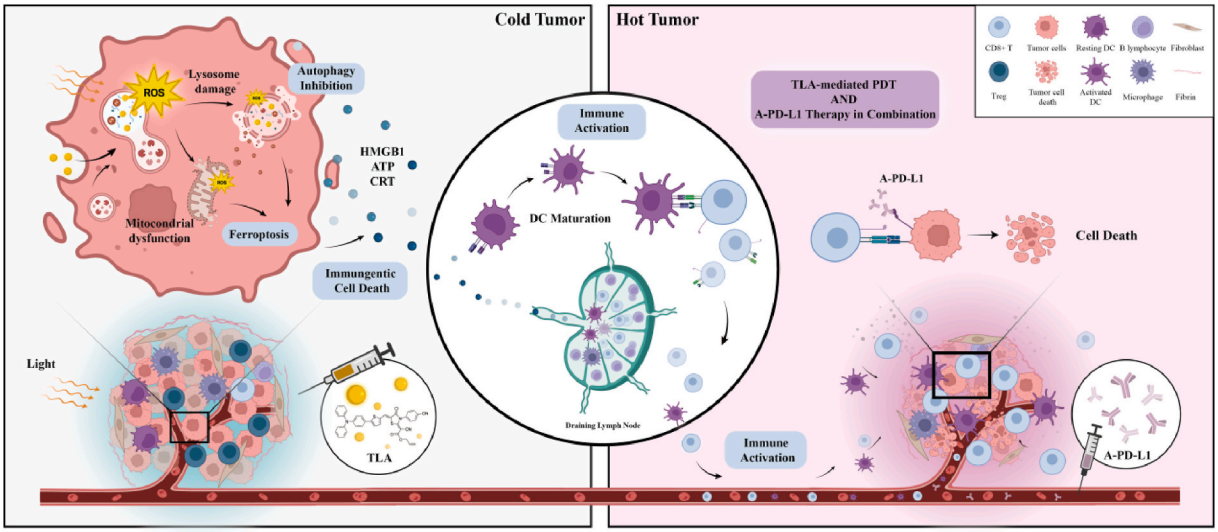

Scheme 1. Schematic illustration of TLA for amplifying anti-tumor immune response. In detail, TLA with light irradiation would trigger lysosome damage and autophagy inhibition, followed by induce mitochondrial damage and ferroptosis occurs, and finally remodel the immunosuppressive microenvironment through the release of DAMPs.

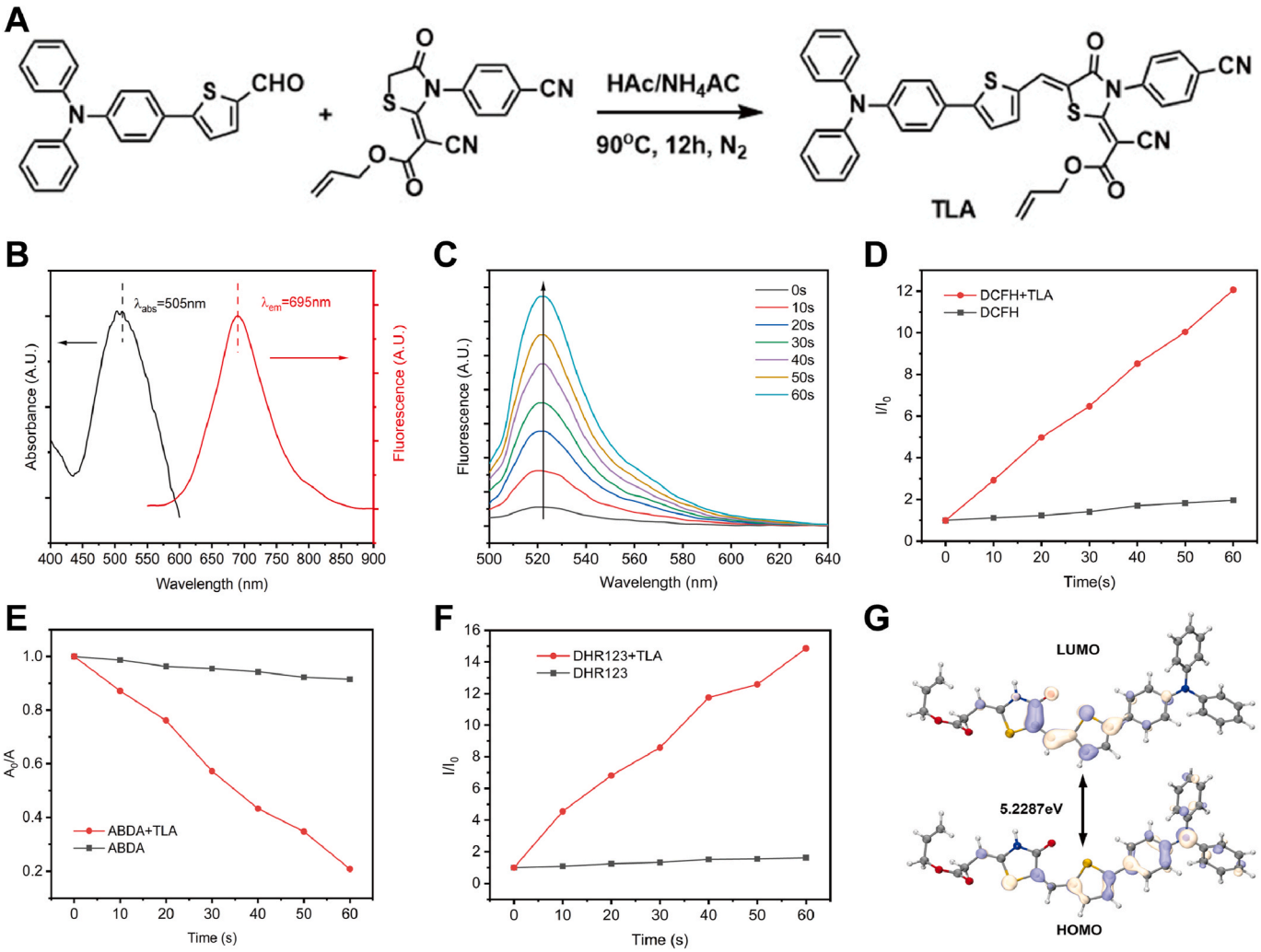

Fig. 1. Synthesis and physical properties of TLA. (A) The synthetic routine of TLA. (B) The UV absorption and fluorescent spectra of TLA. (C) Fluorescence spectra of DCFH with TLA under LED white light irradiation (60 mW/cm^2). (D) The Time-dependent fluorescent change of DCFH with TLA aqueous solution upon white light irradiation (60 mW/cm^2). (E) The Time-dependent absorption change of ABDA upon white light irradiation (60 mW/cm^2). (F) Evaluation of $O_2^{\bullet-}$ generation with fluorescent enhancement of DHR123 for TLA upon white light irradiation (60 mW/cm^2). (G) The optimized molecular conformations and molecular orbitals calculated by density functional theory (DFT).

As depicted in Fig. 1F and Fig. S8 (Supporting Information), there was an obvious fluorescence amplification of DHR 123 when TLA was present with white light irradiation, which indicates the production of $O_2^{\bullet-}$. However, when we used hydroxyphenyl fluorescein (HPF) as the specific indicators for •OH (Fig. S9, Supporting Information), no further ROS were detected. All of these findings supported the notion that TLA demonstrated notable ROS production efficiency, including type-II ROS ($^1O_2$) and type-I ROS ($O_2^{\bullet-}$).

Furthermore, to explore the excited-state property and photophysics of TLA, we carried out theoretical calculations. As shown in Fig. 1G, the delocalized electron density of the HOMO is distributed in the triphenylamine segment, whereas that of the LUMO is primarily concentrated on the Rhodium unit, confirming strong intramolecular charge transfer (ICT) in TLA. Furthermore, TLA exhibited a narrow energy gap between the S1 and T1 states ($\Delta E_{S1\text{-}T1}$ = 1.407 eV) (Fig. S10, Supporting Information), which could improve the capacity to produce ROS.

2.2. TLA-mediated PDT causes lysosome damage and autophagy inhibition

As the physicochemical characteristics results identified that TLA exhibited excellent PDT effect, we further performed cell counting kit-8 (CCK-8) assay to determine the cell viability of CT26 cells after various treatment. As shown in Fig. 2A, our results revealed that TLA had great bio-compatibility and adequate safety in the absence of irradiation. At the same time, cell viability decreased to less than 40 % incubation with 50 μM TLA and irradiation (60 mW/cm^2, 10 min), confirming that TLA may be practical for light-triggered therapy (Fig. 2B). Inspired by the excellent ROS generation ability of TLA under white light, we then applied DCFH-DA probe to examine TLA-induced ROS burst. From the results of flow cytometry, no obvious fluorescence signal was detected in PBS group, free TLA group or Light group. Only in the presence of both TLA and light did the green fluorescence intensity increase significantly (Fig. 2C; Fig. S11, Supporting Information). Meanwhile, the results of CLSM also confirmed that with the addition of light irradiation, TLA treatment could significantly increase intracellular ROS level (Fig. 2D). Collectively, these results highlighted the excellent photo-therapeutic performance of TLA, which would be a potential PDT platform for tumor therapy.

To confirm the localization and evaluate the biological characteristics of TLA in living cells, we firstly carried out a co-localization analysis by incubating CT26 cells with TLA, DAPI and LysoSensor green probe (a commercial probe for lysosomal imaging). As shown in Fig. 2E, TLA could permeated through cell membrane and specifically accumulates in

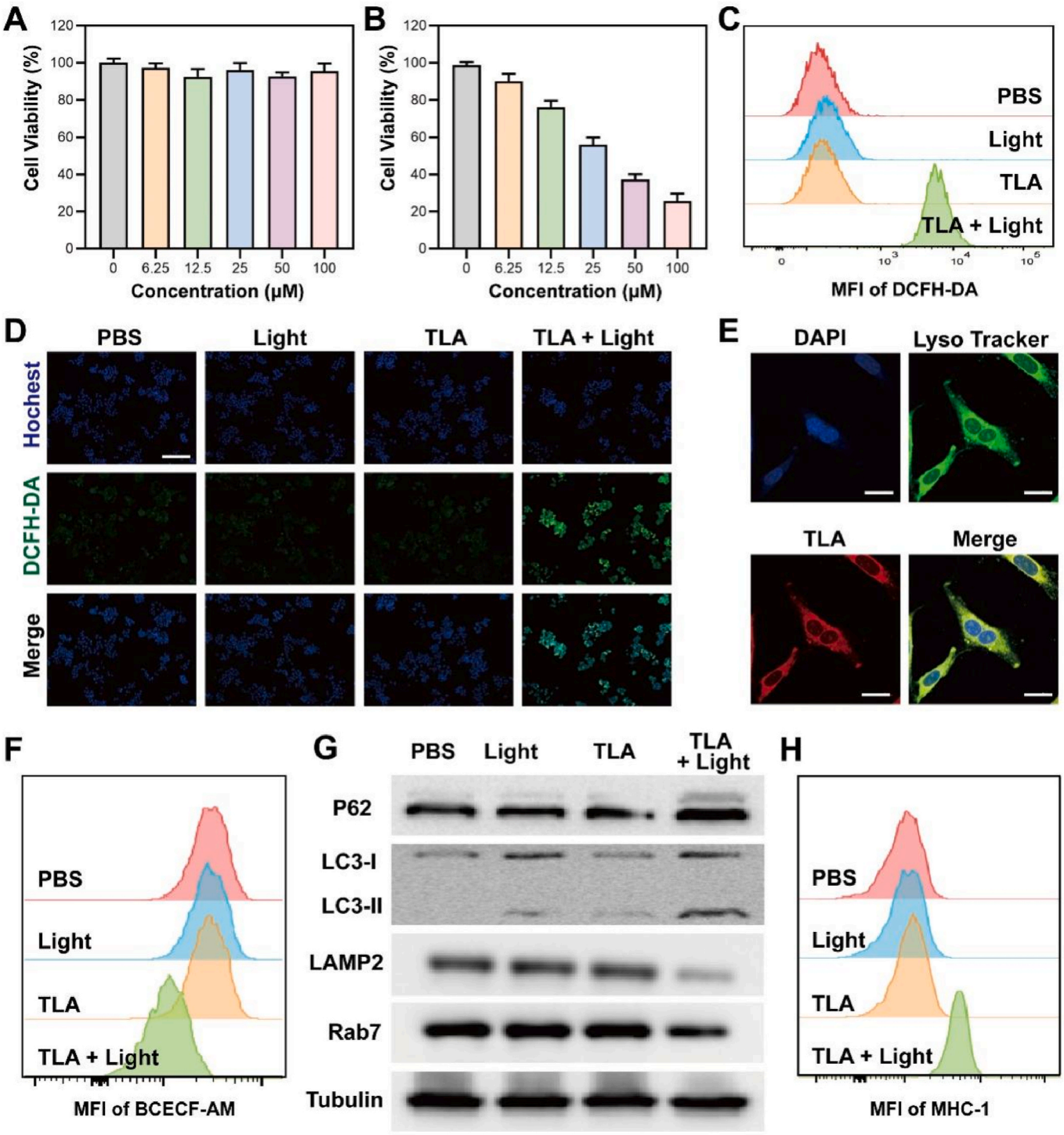

Fig. 2. Lysosome-targeted autophagy inhibition by TLA-mediated PDT. (A) Cytotoxicity of CT26 cells after treated TLA without light irradiation. (B) Cytotoxicity of CT26 cells after treated TLA with light irradiation (60 mW/cm^2, 10 min). (C) Flow cytometric analysis and (D) fluorescent images of intracellular ROS level stained with DCFH-DA probe (Scale bar, 200 μm). (E) Co-localization images of CT26 cells co-stained by TLA, DAPI, and LysoTracker Green, and the Pearson's correlation coefficient denoting the goodness of co-localization, scale bar: 20 μm. (F) Flow cytometric images of cancer cells stained by BCECF-AM for detecting intracellular pH, and relative statistical analysis. (G) Expressions of p62, LC3, LAMP2, and Rab7 in CT26 cells detected by WB after different treatment. (H) Flow cytometric analysis of MHC-I expression within CT26 cells after various treatment.

lysosome. The Pearson's coefficient of the co-location experiment was high (0.93). As mentioned above, ROS-induced oxidative damage by TLA under light irradiation may destroy the membrane integrity of lysosome, and induce following lysosomal membrane permeabilization (LMP). Once the occurrence of LMP, one of the first hallmarks of lysosomal dysfunction, is the release of protons into the cytoplasm to trigger intracellular acidification, which is detrimental to the cells [26,27]. To determine whether TLA with Light activation could affect intracellular acidity, we measured the intracellular pH of cancer cells by a commercial pH indicator (BCECF-AM). As shown in Fig. 2F, the lower green fluorescence signal was only observed in cells incubated with TLA under NIR light irradiation and not in cells incubated with TLA or PBS

(Fig. S12, Supporting Information). Such a finding was taken as evidence that NIR light activation of TLA could trigger intracellular acidification, which attributed to lysosomal dysfunction.

As we all known, lysosome is the main organelle for protective autophagy [28,29]. To determine that autophagy inhibition caused by PDT-induced ROS eruptions are the mechanism responsible for increased cytotoxicity, we analyzed the levels of autophagy-associated proteins via western blot (WB) analysis. Autophagy can be simply divided into four steps: the formation of (i) phagophore, (ii) autophagosomes, (iii) autolysosome and (iv) the degradation of the cargo. P62 (also known as SQSTM1) is a specific receptor protein that mediates the docking of ubiquitinated protein aggregates with autophagosomes, which was subsequently degraded during autophagy. LC3 protein participates in the expanding of phagophore and the formation of an autophagosome [30,31]. In TLA + NIR group, increased LC3-II/LC3-I and elevated levels of P62 indicated an impairment of the autophagy flux, a condition known as autophagic block (Fig. 2G). As to which step in autophagy flux is blocked, we can see that the expression of LAMP2 obviously decreased while the expression of Rab7 only slightly decreased (Fig. 2G). In fact, Rab7 locates on endosome and regulates traffic from early to late endosomes and from late endosome to lysosome; while LAMP-2, is a major protein component of the lysosomal membrane, which can protect the membrane from enzymatic hydrolysis and considered as definitions of the lysosomal compartment. Therefore, this expression changes of LAMP2 and Rab7 in cells suggested that lysosome was damage, while the formation and transport of endosome

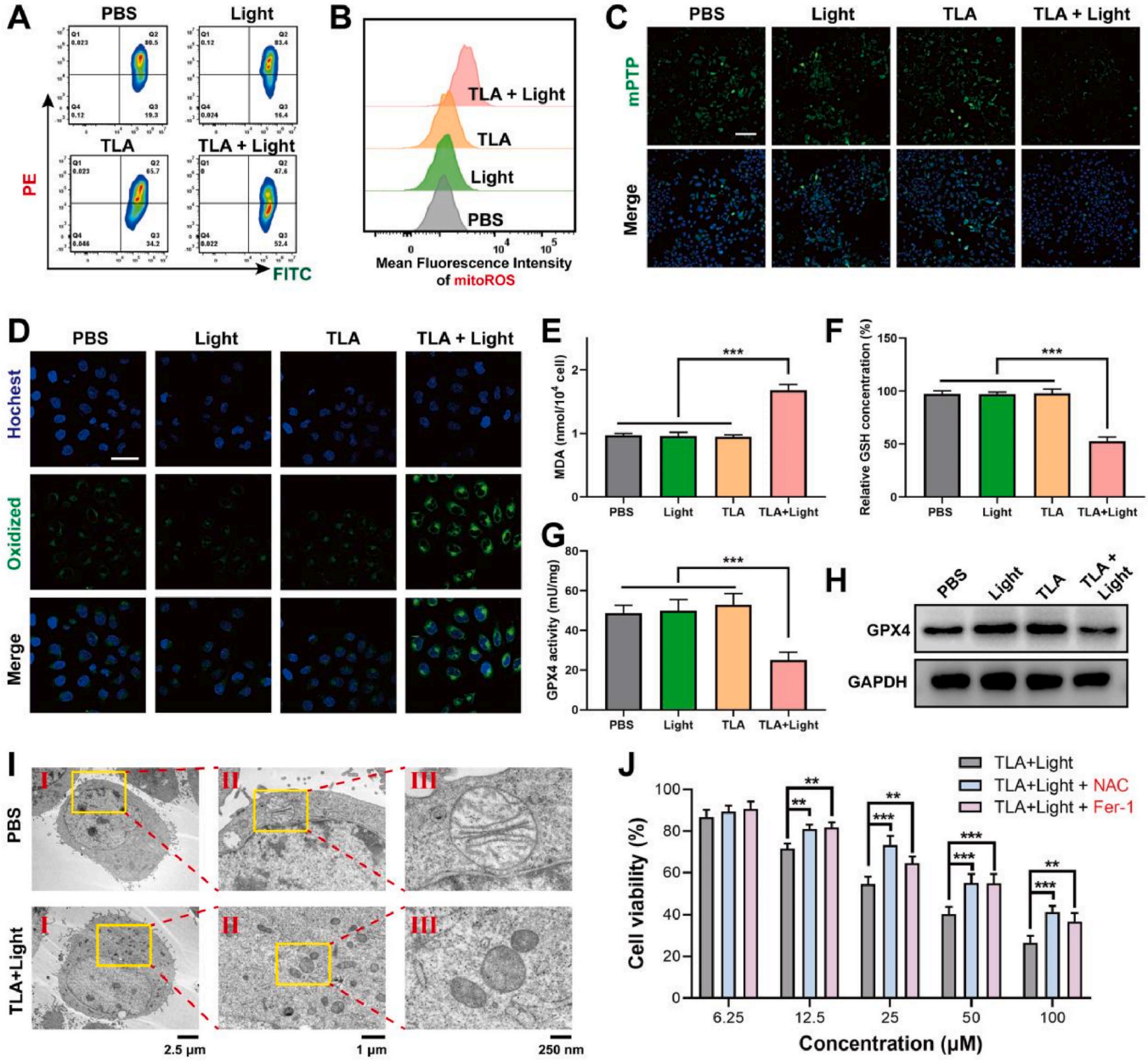

Fig. 3. TLA-mediated PDT triggers ferroptosis, accompanied by mitochondrial dysfunction and oxidative damage. (A) The mitochondrial membrane potential (ΔΨm) in CT26 cells receiving different treatments detected with JC-1 fluorescence probe. (B) Flow cytometry analysis of mitoROS levels in CT26 cells after treating with TLA detected with MitoSOX after different treatments. (C) Mitochondrial permeability transition pore (mPTP) was detected by CLSM, scale bar: 100 μm. (D) CLSM images of CT26 cells using BODIPY581/591-C11 probe to investigate LPO levels, scale bar: 30 μm. (E) Intracellular MDA content. (F) Detection of GSH level of CT26 cells after various treatment. (G) Evaluation of GPX4 activity within CT26 cells. (H) GPX4 protein levels was detected by WB assay. (I) Bio-TEM image of CT26 cell (I) and its local view (II, III) after treatment with TLA + Light. (J) Relative cell viability of CT26 cells after being incubated with NAC or Fer-1. $^{**}P < 0.01$, $^{***}P < 0.001$.

were not much affected. So, the third step of autophagy was blocked.

Emerging studies identified that the tumor cells can evade immune system through autophagy, in which MHC-I was engulfed and then transported to lysosome for biodegradation, leading to compromised T-cell immune response [32]. In this reason, we further determine the intracellular MHC-I level after various treatment. As shown in Fig. 2H, the mean fluorescence intensity (MFI) of MHC-I in CT26 cells of TLA + Light group was significantly increased, indicating improved antigen presentation and immune recognition (Fig. S13, Supporting Information). In summary, following the demonstration that TLA-mediated PDT could specially target lysosomes, trigger ROS storm and cause lysosomal damage, and finally inhibit protective autophagy.

2.3. TLA-mediated PDT triggers ferroptosis, accompanied by mitochondrial dysfunction and oxidative damage

Accumulating evidences suggested that lysosome-targeted photodynamic materials exhibited additional ferroptosis-promoting effect in tumor cells more than ROS induced cellular damage [17,32,33]. LMP induces the release of considerable substances into the cytoplasm, such as proton and irons, which initiate or amplify cell death signaling in the context of ferroptosis [34,35]. Mitochondrial dysfunction is a critical marker of ferroptosis [36,37]. Ferroptosis cells usually exhibit dissipated mitochondrial membrane potential (MMP), increased mitochondrial membrane permeability, and disrupted mitochondrial structure. The MMP is generated in the process of energy metabolism and essential for maintaining mitochondrial function. We investigated MMP with JC-1 by flow cytometry analysis. JC-1 aggregates in the mitochondrial matrix with red fluorescence at high MMP detected in PE panel, and JC-1 monomer with green fluorescence at low MMP detected in FITC panel. As shown in Fig. 3A, cells showed little red fluorescence in the TLA plus light group, indicating the MMP decreased after PDT treatment (Fig. S14, Supporting Information).

Then, the results of flow cytometry revealed that, after treated with TLA plus light irradiation, the intracellular mitoROS level was significantly increased (Fig. 3B; Fig. S15, Supporting Information). Furthermore, mitochondrial membrane permeability was assessed by mitochondrial permeability transition pore (mPTP) detection kit, which is a putative pore-like structure responsible for the induction of mitochondrial permeability transition and cell death. With mPTP probe, we detected that mPTP opening greatly increased as green fluorescence decreased within CT26 cells after PDT treatment, indicating the permeability of mitochondrial membrane was increased (Fig. 3C; Fig. S16, Supporting Information).

The generated ROS and subsequent hydroxyl radical (·OH)-mediated LPO with plasma membrane damage are the core events leading to ferroptosis. To ascertain that the mitochondrial damage was mediated by ferroptosis, experiments were performed to measure the oxidative damage and LPO. Herein, the intracellular LPO levels were detected by BODIPY581/591-C11 probe. As demonstrated in Fig. 3D, the TLA + Light group exhibits stronger green fluorescence, indicating that TLA-mediated PDT effect could evoke ferroptosis through triggering mitochondrial dysfunction.

Antioxidant defense was also detected during ferroptosis. As intracellular malondialdehyde (MDA) is an important end product of LPO, we firstly measured MDA concentration in CT26 cells with different treatment, and MDA increased obviously in TLA + Light group (Fig. 3E). Additionally, the SLC7A11-GSH-GPX4 pathway is the major antioxidant defense systems for ferroptosis cell death against peroxidation damage of membranes. Notably, the level of GSH also fell by almost 50 % after treated with TLA + Light compared to the control (Fig. 3F). This depletion of GSH was accompanied by a corresponding reduction in the activity of GPX4 and its expression, as measured by ELISA assay and western blotting, respectively (Fig. 3G–H). The bio-TEM images of the CT26 cells treated with TLA + Light demonstrated mitochondrial fragmentation and cristae alterations (Fig. 3I). Besides, it was found that the ferroptosis inhibitors (Fer-1) and the ROS inhibitor acetylcysteine (NAC) both significantly decreased the TLA + Light-induced cytotoxicity (Fig. 3J). In conclusion, all of these studies revealed the notion that during TLA-mediated PDT, ferroptosis was initiated and amplified, accompanied with mitochondrial dysfunction and imbalance of oxidation and antioxidation.

2.4. TLA-mediated PDT elicits ICD and promotes DCs maturation in vitro

Multiple PDT-based tumor suppressors have been shown to sensitize cells to ferroptosis, as well as enhance an immune response, with more DC maturation and T lymphocytes infiltration [38–40]. Correspondingly, emerging studies suggested that membrane disruption by ferroptosis cause inflammation and induce a release of endogenous DAMPs [41,42]. Therefore, a reasonable hypothesis is that the onset of ferroptosis results in the activation of immune cells and ICD.

Key DAMPs exposed during ICD include calreticulin (CRT), high mobility group box 1 (HMGB1), adenosine triphosphate (ATP). They act as an “eat me” signal to antigen presenting cells, which lead to initiate anti-tumor immune response. As shown in Fig. 4A, compared with the cells in PBS group, CT26 cells treated with free NIR or TLA exhibit similar green fluorescence intensity, and obviously lower fluorescence intensity is observed in TLA + Light group. Additionally, emerging studies identified that surface-exposed CRT had been widely used to detect the process of ICD [43]. As indicated in Fig. 4B, CT26 cells treated with TLA exhibit significantly enhanced green fluorescence after exposure to Light irradiation, suggesting an elevated amount of CRT on the CT26 cell surface. Meanwhile, the results of flow cytometry in Fig. 4C also exhibited a similar result (Fig. S17, Supporting Information). Moreover, we further examined the level of environmental HMGB1 and ATP through ELISA assay, and both were remarkably increased in the culture supernatant of CT26 cells treated with TLA + Light (Fig. 4D–E). These results confirmed the notion that endogenous DAMPs were released by tumor cells during the process of ferroptosis under TLA + Light treatment.

As DAMPs released during ICD are firstly recognized by antigen presenting cells, especially DCs, we studied DC maturation in vitro using Transwell devices. Then, the maturity level of collected DCs was tested using flow cytometry, and the secretion of cytokines was detected using the enzyme-linked immunosorbent assay (ELISA). Correspondingly, the PDT treated tumor cells significantly induced the maturation of DCs from the flow cytometry analysis, and the DC maturation rates increased to 24 %, compared with 6.63 % in PBS group (Fig. 4F). As indicated in Fig. S18 (Supporting Information), after treated with TLA + Light, the secretion of immune-related cytokines TNF-α and IL-6 were both significantly increased, which further confirmed that TLA could induce DC activation and maturation. The results above supported our hypothesis that, ferroptosis triggered by TLA + Light, may be a promising strategy to break immunological tolerance.

2.5. TLA-mediated PDT exhibits capable tumor ablation in vivo

Inspired by the performance of TLA-mediated PDT in vitro, we conducted animal experiment to confirm the efficacy of PDT treatment in subcutaneous colorectal cancer model. Firstly, the Balb/c mice with subcutaneous CT26 tumors were randomly divided into four groups (PBS, TLA, Light, and TLA + Light group) and injected with TLA intratumorally at a dose of 0.5 mg/kg body weight. Then, the tumor was irradiated with white light at 6h post-injection at 60 mW/cm^2 for 10 min (Fig. 5A). As shown in Fig. 5B–C, the tumor size and tumor weight increased rapidly in PBS group. In comparison, TLA + Light showed remarkable tumor growth inhibition due to TLA-mediated PDT effect.

Notably, there was no significant change in the body weight of the mice during the whole treatment, indicating the bio-safety of the TLA (Fig. 5D). Additionally, the biocompatibility of TLA was examined to confirm the safety of TLA, considering the long retention time in vivo.

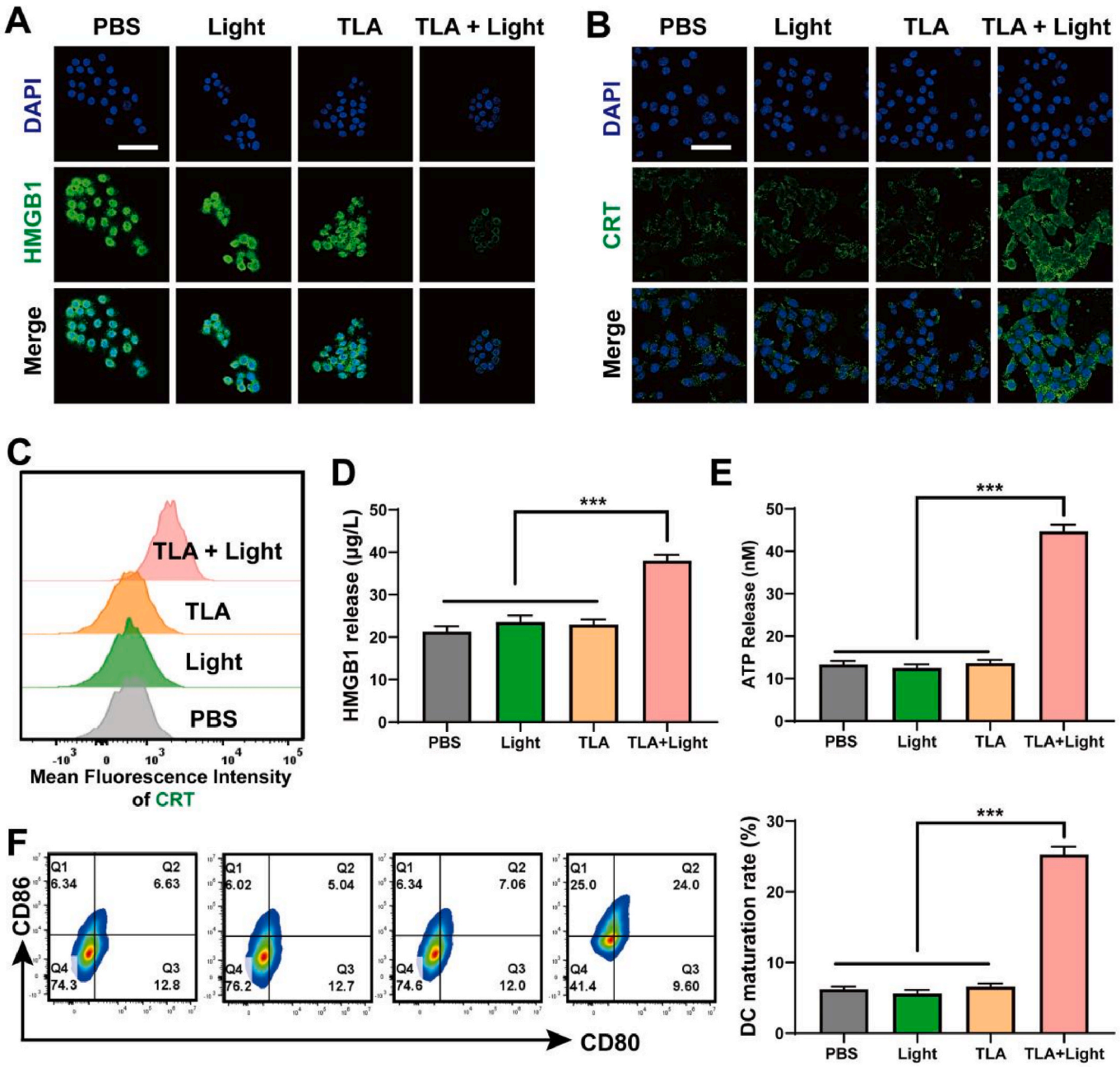

Fig. 4. TLA-mediated PDT induces ICD and promoted DCs maturation in vitro. (A) HMGB1 and (B) CRT expression of CT26 cells after various treatment detected by CLSM, scale bar: 40 μm. (C) MFI of CRT expression of CT26 cells by flow cytometry. (D) HMGB1 and (E) ATP concentration in medium of CT26 cells after various treatments. (F) Flow cytometry of matured DCs ($CD80^+CD86^+$) after incubation with CT26 cells receiving different treatments. $^*P < 0.05$, $^{**}P < 0.01$, $^{***}P < 0.001$.

TLA was injected intravenously into mice. Compared with PBSgroup, H&E images of heart, liver, spleen, lung, and kidney of mice harvested showed no apparent histopathological abnormalities (Fig. S19, Supporting Information). These results confirmed the low toxicity and good biocompatibility of TLA.

Moreover, the ELISA results also displayed that the secretion levels of immunostimulatory cytokines including IL-6, TNF-α, and interferon γ (IFN-γ) in PDT group was significantly increased relative to other groups (Fig. 5E–G). In order to further determine the therapeutic effect, we collected the tumor tissues of the treated mice for H&E staining. As indicated in Fig. 5H, compared with the PBS group, larger damaged area was found in the tumor tissues of TLA + Light group. Correspondingly, the positive area of TUNEL staining within tumor slices from the TLA + Light groups was also higher than that in other groups, suggesting higher cell death rate (Fig. 5H). Furthermore, as showed in Fig. S20 (Supporting **Information**), immunofluorescence-stained tumor sections also showed that treatment with TLA plus Light could significantly promote CRT expression, which induce ICD occur and activate anti-tumor immune response. Taken together, these results identified that TLA-mediated PDT effect could effectively inhibit colorectal cancer growth.

2.6. TLA-mediated PDT induces immune activation and TME reprogrammed in vivo

Based on our in vitro research, TLA-mediated PDT promoted DC maturation and might break immunological tolerance by initiating ICD effect. This discovery prompted us to evaluate the in vivo activation of immune cells and the remodeling of TME under PDT therapy. We

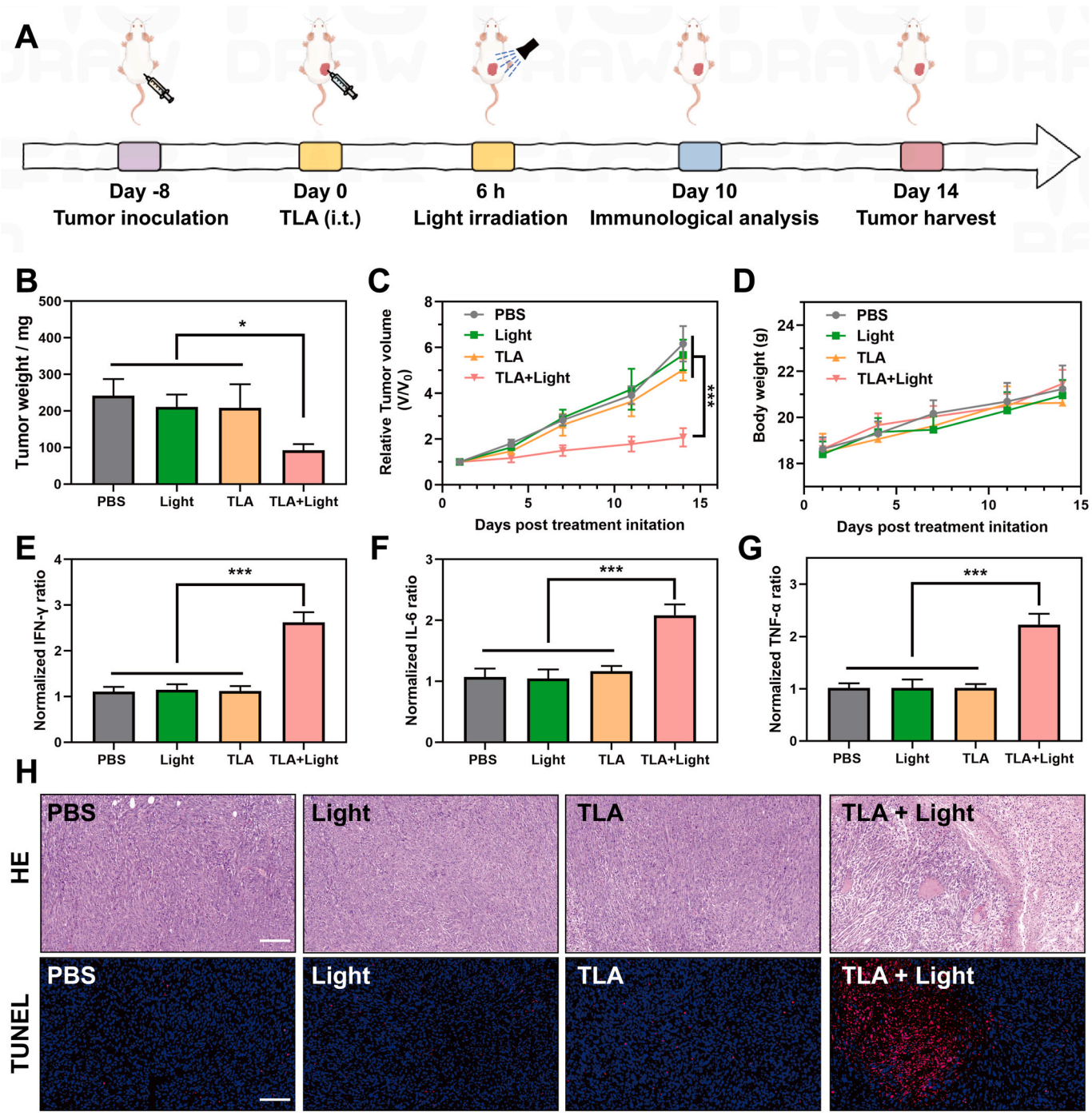

Fig. 5. TLA-mediated PDT exhibits capable in vivo tumor ablation. (A) Timeline illustrating the construction of CT26-tumor bearing mice model and therapeutic process. (B) Tumor weight, (C) relative tumor volume and (D) body weight changes after various treatment. (E–G) The cytokines of IFN-γ, IL-6, and TNF-α in the serum of mice evaluated using ELISA. (H) H&E and TUNEL staining of dissected tumor tissues, scale bar: 150 μm $^{**}P < 0.01$, $^{***}P < 0.001$.

performed animal experiments and the animal models were constructed, grouped, treated as previously described. After 10 days, mice were sacrificed, and the tumor tissues, lymph nodes and spleen tissues were isolated and detected by Flow Cytometry. Consistence with the results of in vitro experiment, the DC maturation rate ($CD45^+CD11c^+CD80^+CD86^+$) in TLA + Light group significantly increased to 34.7 %, approximately twice that of the other three groups, indicating its better antigen cognization and presentation ability (Fig. 6A and E).

Since T lymphocytes exhibit direct tumor cell ablation, we investigated the recruitment and activation of tumor-infiltrating T lymphocytes. From the result of Flow Cytometry assay, mice treated with TLA + Light enhanced intra-tumoral infiltration of cytotoxic T lymphocytes (CTLs, $CD45^+CD3^+CD8^+$), and the population of tumor infiltrating CTLs was ~1.90-fold higher than that in PBS control group (2.76 %) (Fig. 6B and F). Then, the proportion of T cell subsets was further analyzed. A remarkable increase of effector T lymphocytes ($CD45^+CD3^+CD8^+GZMB^+$) in the tumor was observed in the TLA + Light group (30.6 %), compared with those in the PBS group (21.8 %), Light group (22.8 %), and TLA group (24.4 %), indicating increased release of tumor-killing molecules (Fig. 6D and H). Emerging studies identified that central memory T cells (T_{CM}) have strong proliferation

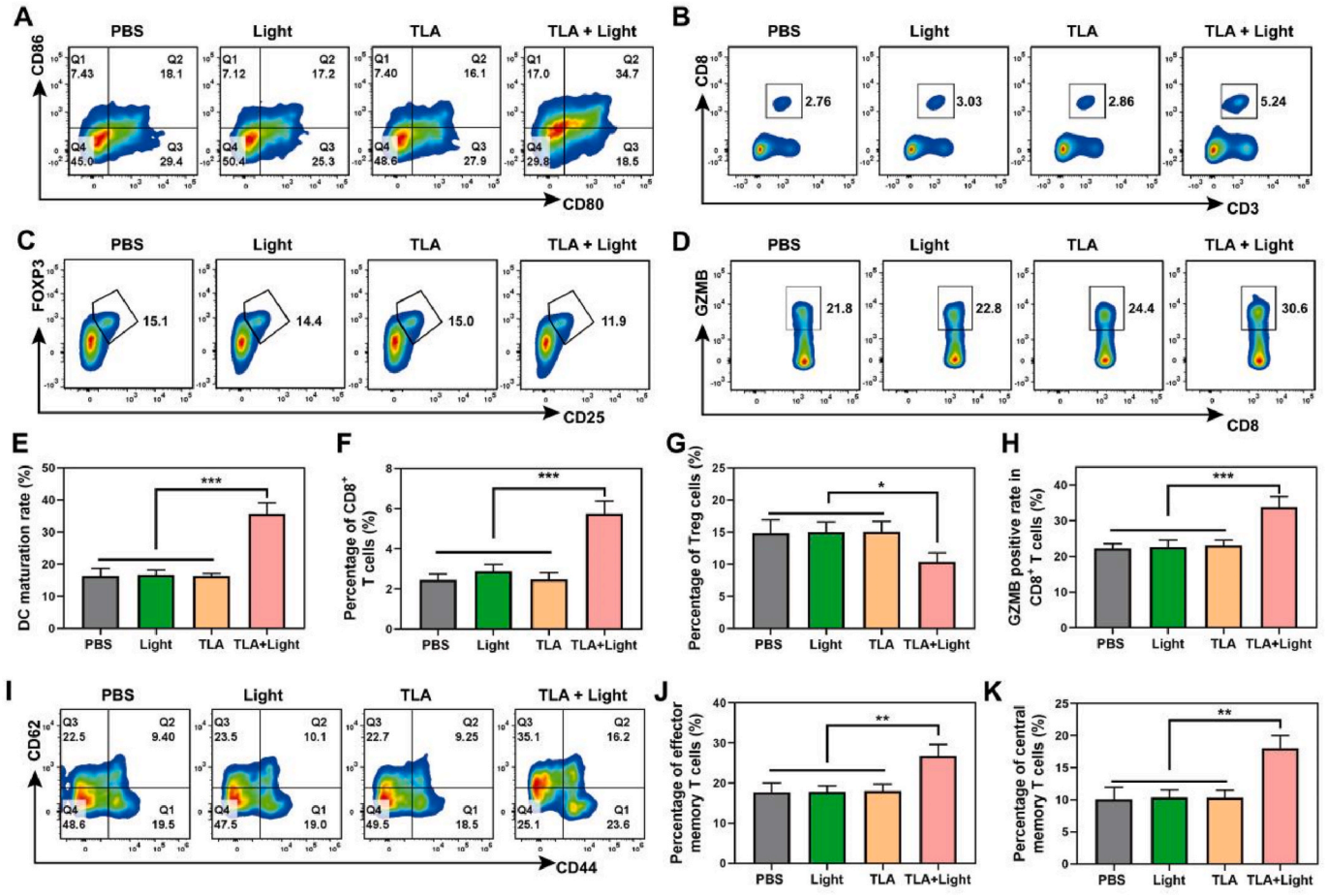

Fig. 6. TLA-mediated PDT induces immune activation and TME reprogramming in vivo. (A) Representative flow cytometry plots of maturated DCs ($CD11c^+CD80^+CD86^+$) in the lymph nodes. (B) Representative flow cytometry plots of $CD8^+$ T cells ($CD3^+CD8^+$), (C) Tregs cells ($CD4^+CD25^+FoxP3^+$) and (D) CTLs ($CD3^+CD8^+GZMB^+$) within the tumor tissues. (E–H) quantitative analysis for the percentage of matured DC cells, $CD8^+$ T cells, Tregs cells and CTLs, respectively. (I–K) Representative flow cytometry plots and quantitative analysis of T_{EM} and T_{CM} cells in the spleen tissues. $^*P < 0.05$, $^{**}P < 0.01$, $^{***}P < 0.001$.

and maintain long-term protection against re-infection, while effector memory T cells (T_{EM}) mainly provide the first-line immune defense and trigger immediate protection. Herein, the fraction of T_{CM} and T_{EM} cells within spleen tissues of mice in the TLA + Light group are significantly higher than those in the other groups (Fig. 6I–K). Additionally, the amount of inhibitory Tregs ($CD4^+CD25^+Foxp3^+$) in the tumors from the TLA + Light group was significantly decreased to 11.9 %, only almost two-third of that in the PBS group (15.1 %) (Fig. 6C and G). In summary, these above results confirmed that TLA-mediated PDT could trigger DCs maturation, promote T cell recruitment, and generate a strong tumor-specific T cell response with remodeled TME in vivo.

2.7. TLA-mediated PDT effectively synergizes with A-PD-L1 therapy

As we have demonstrated, TLA-mediated PDT could amplify the effect of ferroptosis through lysosome-targeted autophagy inhibition, inducing ICD and anti-tumor immune activation. However, accumulated studies identified that the PDT effect could trigger the release of IFN-γ, which contributed to PD-L1 upregulation and induce immunologic escape. To overcome the above limitation, we next performed combinatory therapy by TLA + Light and A-PD-L1 in Balb/c mice (Fig. 7A). In brief, the model mice were randomly divided into four groups (PBS, A-PD-L1, TLA + Light, TLA + Light + A-PD-L1 group), and the therapeutic efficacy of respective treatments was evaluated through monitoring tumor volumes and tumor weights. As shown in Fig. 7C, the tumors grew rapidly in PBS-treated mice, and the treatment of A-PD-L1 alone display a moderate tumor suppression effect after 14 days. In contrast, the combined treatment of tumors with TLA + Light and A-PD-L1 could further more significantly inhibit tumor growth than other groups (Fig. 7C). Besides the tumor weight change, we also monitored the tumor volume change in different treatment groups (Fig. 7B), and confirmed the perfect antitumor efficacy of the TLA + Light and A-PD-L1. When mice were sacrificed, tumor infiltrating immune cells were isolated and analyzed with flow cytometry. As we can see in Fig. 7D–E, mice went through PDT + A-PD-L1 combinational had more tumor infiltrating CD8 T lymphocytes, at a ratio of 7.53 %, compared with control group (2.45 %), A-PD-L1 group (3.56 %), and PDT group (5.65 %). Furthermore, in order to determine the treatment mechanism based on tumor pathological analysis, the dissected tumor tissues were further stained with H&E. As shown in Fig. 7F, the H&E and TUNEL staining results show serious injury of tumor cells in combinational treatment group relative to other groups. Taken together, the results highlighted the potency of TLA + Light + A-PD-L1 combinational therapy for cancer treatment and provided a promising therapeutic strategy for immunotherapy-resistant tumors.

3. Conclusion

We have successfully constructed a lysosome targeting photosensitizer TLA. TLA displayed robust light stability, good biocompatibility, high photothermal conversion efficiency, and efficient antitumor performance. Mechanistically, TLA-mediated PDT had great potential to induce and amplify ferroptosis by lysosome damage and autophagy inhibition, thereby promoting tumor ablation and immune activation.

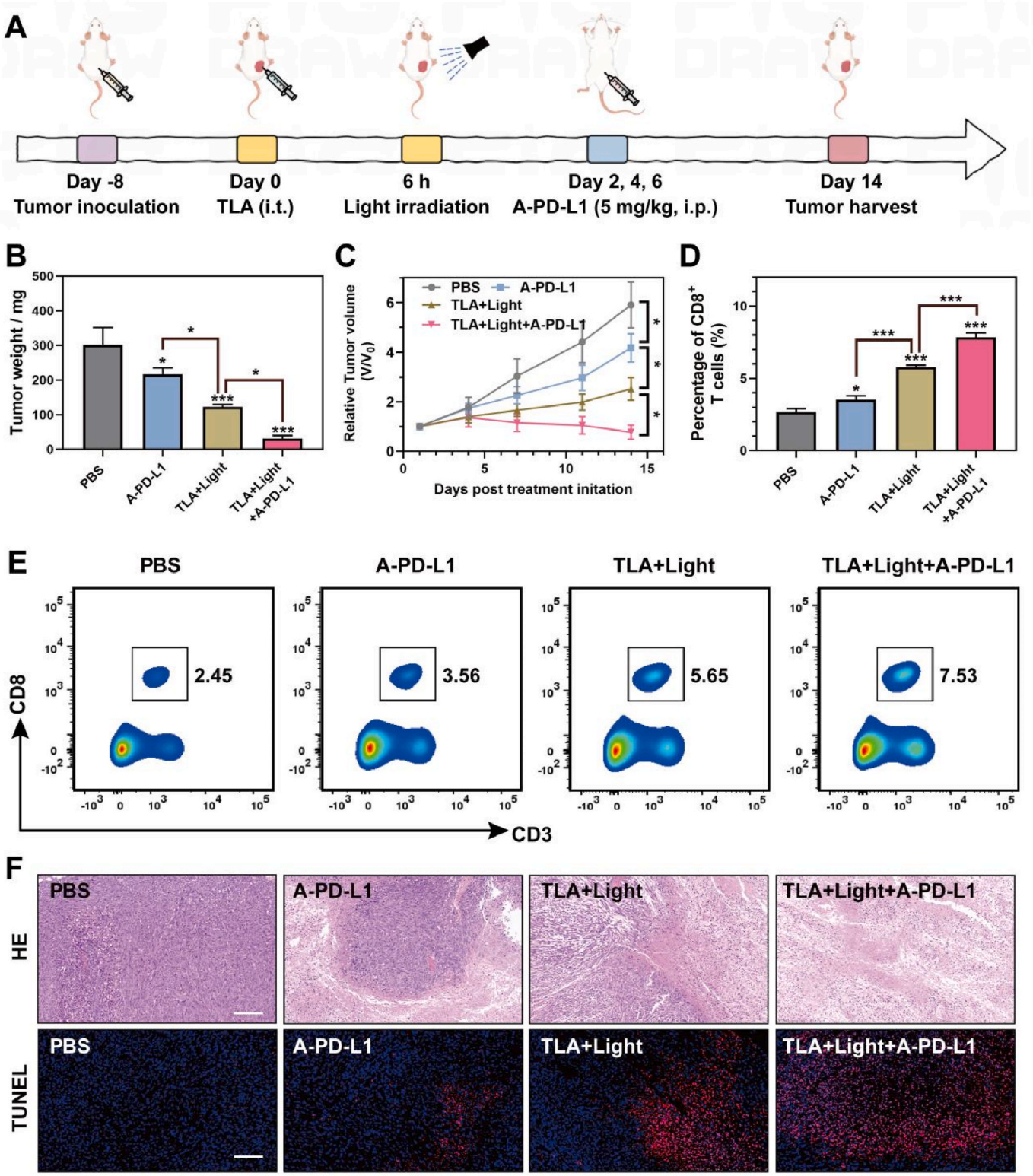

Fig. 7. TLA-mediated PDT effectively synergizes with A-PD-L1 therapy. (A) Therapeutic schedule for the CT26 tumor-bearing mice. (B) Tumor weight, (C) relative tumor volume changes after various treatment. (D–E) Flow Cytometry images and statistical analysis of the percentages of $CD8^+$ T cells in tumor tissues of the mice after different treatments. (F) H&E and TUNEL staining of dissected tumor tissues, scale bar: 150 μm $^*P < 0.05$, $^{**}P < 0.01$, $^{***}P < 0.001$.

Further studies have shown that TLA-mediated PDT could effectively synergize with A-PD-L1 therapy to mediate potent tumor ablation, providing a novel strategy for anti-tumor therapy.

CRediT authorship contribution statement

Zhian Chen: Writing – original draft, Software, Methodology, Formal analysis, Data curation, Conceptualization. **Yutong Wang:** Writing – original draft, Software, Resources, Project administration,

Data curation. **Zhenhao Li:** Writing – original draft, Validation, Investigation, Data curation. **Meijuan Chen:** Software, Resources, Methodology. **Yingshi Li:** Visualization, Validation, Software, Methodology, Investigation. **Chuyue Lu:** Visualization, Methodology, Investigation, Formal analysis, Data curation. **Zhenyu Lin:** Visualization, Validation, Supervision, Software, Resources. **Hua Zheng:** Writing – review & editing, Project administration, Funding acquisition, Formal analysis, Data curation. **Lujia Chen:** Writing – review & editing, Supervision, Resources, Project administration, Data curation. **Qianbing Zhang:** Writing – review & editing, Visualization, Supervision, Project administration, Investigation, Conceptualization.

Declaration of competing interest

The authors declare that they have no known competing financial interests or personal relationships that could have appeared to influence the work reported in this paper.

Acknowledgement

This work was supported by grants from the Natural Science Foundation of Guangdong Province (No. 2024A1515010390), the President Foundation of Nanfang Hospital, Southern Medical University (No. 2023A022), the Medical Scientific Research Foundation of Guangdong Province (No. A2023124).

Appendix A. Supplementary data

Supplementary data to this article can be found online at https://doi.org/10.1016/j.mtbio.2025.101552.

Data availability

Data will be made available on request.

References

[1] R.S. Riley, C.H. June, R. Langer, M.J. Mitchell, Nat. Rev. Drug Discov. 18 (3) (2019) 175–196.
[2] K. Ganesh, Z.K. Stadler, A. Cercek, R.B. Mendelsohn, J. Shia, N.H. Segal, et al., Nat. Rev. Gastroenterol. Hepatol. 16 (6) (2019) 361–375.
[3] M. Al Zein, M. Boukhdoud, H. Shammaa, H. Mouslem, L.M. El Ayoubi, R. Iratni, et al., Drug Discov. Today 28 (9) (2023) 103669.
[4] X. Chen, R. Kang, G. Kroemer, D. Tang, Cell Death Differ. 28 (10) (2021) 2843–2856.
[5] X. Jiang, B.R. Stockwell, M. Conrad, Nat. Rev. Mol. Cell Biol. 22 (4) (2021) 266–282.
[6] Y. Mou, J. Wang, J. Wu, D. He, C. Zhang, C. Duan, et al., J. Hematol. Oncol. 12 (1) (2019) 34.
[7] S. Luo, D. Ma, R. Wei, W. Yao, X. Pang, Y. Wang, et al., Acta Biomater. 138 (2022) 518–527.
[8] M.J. Ko, S. Min, H. Hong, W. Yoo, J. Joo, Y.S. Zhang, et al., Bioact. Mater. 32 (2024) 66–97.
[9] L. Xie, J. Li, G. Wang, W. Sang, M. Xu, W. Li, et al., J. Am. Chem. Soc. 144 (2) (2022) 787–797.
[10] W. Guo, Z. Chen, Z. Li, H. Huang, Y. Ren, Z. Li, et al., Chem. Eng. J. 455 (2023) 140868.
[11] H. Liang, X. Wu, G. Zhao, K. Feng, K. Ni, X. Sun, J. Am. Chem. Soc. 143 (38) (2021) 15812–15823.
[12] C. Liang, X. Zhang, M. Yang, X. Dong, Advanced materials (Deerfield Beach, Fla) 31 (51) (2019) e1904197.
[13] D.W. Zheng, Q. Lei, J.Y. Zhu, J.X. Fan, C.X. Li, C. Li, et al., Nano Lett. 17 (1) (2017) 284–291.
[14] Q. Feng, W. Fang, Y. Guo, P. Hu, J. Shi, J. Am. Chem. Soc. 145 (44) (2023) 24153–24165.
[15] Q. Guan, L.L. Zhou, Y.B. Dong, J. Mater. Chem. B 9 (43) (2021) 8906–8936.
[16] D. Tang, R. Kang, T.V. Berghe, P. Vandenabeele, G. Kroemer, Cell Res. 29 (5) (2019) 347–364.
[17] W. Li, S. Yin, Y. Shen, H. Li, L. Yuan, X.B. Zhang, J. Am. Chem. Soc. 145 (6) (2023) 3736–3747.
[18] X. Wei, Y. Li, H. Chen, R. Gao, P. Ning, Y. Wang, et al., Adv. Sci. 11 (9) (2024) e2302093.
[19] F. Rizzollo, S. More, P. Vangheluwe, P. Agostinis, Trends Biochem. Sci. 46 (12) (2021) 960–975.
[20] M. Wang, C. Yang, M. Chang, Y. Xie, G. Zhu, Y. Qian, et al., Nano Today 52 (2023) 101981.
[21] T. Kurz, U.T. Brunk, Autophagy of HSP70 and chelation of lysosomal iron in a non-redox-active form, Autophagy 5 (1) (2009) 93–95.
[22] C. Ullio, U.T. Brunk, C. Urani, P. Melchioretto, G. Bonelli, F.M. Baccino, et al., Autophagy 11 (12) (2015) 2184–2198.
[23] M. Buccarelli, M. Marconi, S. Pacioni, I. De Pascalis, Q.G. D'Alessandris, M. Martini, et al., Cell Death Dis. 9 (8) (2018) 841.
[24] Q. Xiong, X. Li, W. Li, G. Chen, H. Xiao, P. Li, et al., Front. Mol. Biosci. 8 (2021) 645831.
[25] D. Zhang, J. Yang, S. Ye, Y. Wang, C. Liu, Q. Zhang, et al., Small (Weinheim an der Bergstrasse, Germany) 18 (13) (2022) e2107071.
[26] M. Ghosh, F. Carlsson, A. Laskar, X.M. Yuan, W. Li, FEBS Lett. 585 (4) (2011) 623–629.
[27] W. Bao, M. Liu, J. Meng, S. Liu, S. Wang, R. Jia, et al., Nat. Commun. 12 (1) (2021) 6399.
[28] Q. Xu, H. Zhang, H. Liu, Y. Han, W. Qiu, Z. Li, Biomaterials 280 (2022) 121287.
[29] Y. Yang, Q. Wang, D. Song, R. Zen, L. Zhang, Y. Wang, et al., Journal of experimental & clinical cancer research : CR 39 (1) (2020) 197.
[30] J.M.M. Levy, C.G. Towers, A. Thorburn, Nat. Rev. Cancer 17 (9) (2017) 528–542.
[31] D. Glick, S. Barth, K.F. Macleod, J. Pathol. 221 (1) (2010) 3–12.
[32] H. Xiao, X. Li, B. Li, S. Yang, J. Qin, S. Han, et al., Small 19 (30) (2023) e2300280.
[33] Y. Yan, J. Chen, M. Peng, X. Zhang, E. Feng, Q. Li, et al., Phytochemistry 214 (2023) 113805.
[34] A. Terman, T. Kurz, Antioxidants Redox Signal. 18 (8) (2013) 888–898.
[35] S. Torii, R. Shintoku, C. Kubota, M. Yaegashi, R. Torii, M. Sasaki, et al., The Biochemical journal 473 (6) (2016) 769–777.
[36] B. Gan, The Journal of cell biology 220 (9) (2021) e202105043.
[37] B. Qiu, F. Zandkarimi, C.T. Bezjian, E. Reznik, R.K. Soni, W. Gu, et al., Cell 187 (5) (2024) 1177–1190.e1118.
[38] W. Guo, Z. Chen, Z. Li, H. Huang, Y. Ren, B. Zhao, et al., Chem. Eng. J. 443 (2022) 136428.
[39] Z.W. Qiu, Y.T. Zhong, Z.M. Lu, N. Yan, R.J. Kong, J.Q. Huang, et al., ACS Nano 18 (13) (2024) 9713–9735.
[40] D. Ding, H. Zhong, R. Liang, T. Lan, X. Zhu, S. Huang, et al., Adv. Sci. 8 (14) (2021) 2100712.
[41] X. Niu, L. Chen, Y. Li, Z. Hu, F. He, Seminars in cancer biology 86 (Pt 3) (2022) 273–285.
[42] J. Liu, J. Zhan, Y. Zhang, L. Huang, J. Yang, J. Feng, et al., Advanced materials (Deerfield Beach, Fla) 36 (9) (2024) e2309562.
[43] A. Ahmed, S.W.G. Tait, Mol. Oncol. 14 (12) (2020) 2994–3006.